Time-Dependent CP-Violating Asymmetry in $B^0 \to \rho^0\gamma$ Decays

Y. Ushiroda,[7] K. Sumisawa,[7] N. Taniguchi,[16] I. Adachi,[7] H. Aihara,[42] K. Arinstein,[1] T. Aushev,[18,12] S. Bahinipati,[3] A. M. Bakich,[38] V. Balagura,[12] E. Barberio,[21] K. Belous,[11] U. Bitenc,[13] A. Bondar,[1] A. Bozek,[27] M. Bračko,[20,13] T. E. Browder,[6] P. Chang,[26] Y. Chao,[26] A. Chen,[24] W. T. Chen,[24] B. G. Cheon,[5] R. Chistov,[12] I.-S. Cho,[47] Y. Choi,[37] J. Dalseno,[21] M. Dash,[46] S. Eidelman,[1] D. Epifanov,[1] N. Gabyshev,[1] B. Golob,[19,13] H. Ha,[15] J. Haba,[7] K. Hara,[22] T. Hara,[32] K. Hayasaka,[22] M. Hazumi,[7] D. Heffernan,[32] T. Hokuue,[22] Y. Hoshi,[40] W.-S. Hou,[26] H. J. Hyun,[17] K. Inami,[22] A. Ishikawa,[34] H. Ishino,[43] R. Itoh,[7] Y. Iwasaki,[7] D. H. Kah,[17] J. H. Kang,[47] H. Kawai,[2] T. Kawasaki,[29] H. Kichimi,[7] Y. J. Kim,[4] K. Kinoshita,[3] S. Korpar,[20,13] P. Križan,[19,13] P. Krokovny,[7] R. Kumar,[33] C. C. Kuo,[24] A. Kuzmin,[1] Y.-J. Kwon,[47] M. J. Lee,[36] S. E. Lee,[36] T. Lesiak,[27] S.-W. Lin,[26] D. Liventsev,[12] F. Mandl,[10] S. McOnie,[38] T. Medvedeva,[12] K. Miyabayashi,[23] H. Miyake,[32] H. Miyata,[29] Y. Miyazaki,[22] R. Mizuk,[12] D. Mohapatra,[46] G. R. Moloney,[21] Y. Nagasaka,[8] M. Nakao,[7] H. Nakazawa,[24] S. Nishida,[7] O. Nitoh,[45] S. Noguchi,[23] T. Nozaki,[7] S. Ogawa,[39] T. Ohshima,[22] S. Okuno,[14] S. L. Olsen,[6,9] P. Pakhlov,[12] G. Pakhlova,[12] C. W. Park,[37] H. Park,[17] L. S. Peak,[38] L. E. Piilonen,[46] H. Sahoo,[6] Y. Sakai,[7] O. Schneider,[18] J. Schümann,[7] A. J. Schwartz,[3] K. Senyo,[22] M. E. Sevior,[21] M. Shapkin,[11] C. P. Shen,[9] H. Shibuya,[39] J.-G. Shiu,[26] B. Shwartz,[1] J. B. Singh,[33] A. Sokolov,[11] A. Somov,[3] S. Stanič,[30] M. Starič,[13] T. Sumiyoshi,[44] O. Tajima,[7] F. Takasaki,[7] K. Tamai,[7] M. Tanaka,[7] Y. Teramoto,[31] I. Tikhomirov,[12] K. Trabelsi,[7] S. Uehara,[7] K. Ueno,[26] T. Uglov,[12] Y. Unno,[5] S. Uno,[7] P. Urquijo,[21] Y. Usov,[1] G. Varner,[6] K. Vervink,[18] S. Villa,[18] C. C. Wang,[26] C. H. Wang,[25] M.-Z. Wang,[26] P. Wang,[9] X. L. Wang,[9] Y. Watanabe,[14] E. Won,[15] B. D. Yabsley,[38] A. Yamaguchi,[41] Y. Yamashita,[28] M. Yamauchi,[7] Z. P. Zhang,[35] A. Zupanc,[13] and O. Zyukova[1]

(Belle Collaboration)

[1]*Budker Institute of Nuclear Physics, Novosibirsk*
[2]*Chiba University, Chiba*
[3]*University of Cincinnati, Cincinnati, Ohio 45221*
[4]*The Graduate University for Advanced Studies, Hayama*
[5]*Hanyang University, Seoul*
[6]*University of Hawaii, Honolulu, Hawaii 96822*
[7]*High Energy Accelerator Research Organization (KEK), Tsukuba*
[8]*Hiroshima Institute of Technology, Hiroshima*
[9]*Institute of High Energy Physics, Chinese Academy of Sciences, Beijing*
[10]*Institute of High Energy Physics, Vienna*
[11]*Institute of High Energy Physics, Protvino*
[12]*Institute for Theoretical and Experimental Physics, Moscow*
[13]*J. Stefan Institute, Ljubljana*
[14]*Kanagawa University, Yokohama*
[15]*Korea University, Seoul*
[16]*Kyoto University, Kyoto*
[17]*Kyungpook National University, Taegu*
[18]*École Polytechnique Fédérale de Lausanne (EPFL), Lausanne*
[19]*University of Ljubljana, Ljubljana*
[20]*University of Maribor, Maribor*
[21]*University of Melbourne, School of Physics, Victoria 3010*
[22]*Nagoya University, Nagoya*
[23]*Nara Women's University, Nara*
[24]*National Central University, Chung-li*
[25]*National United University, Miao Li*
[26]*Department of Physics, National Taiwan University, Taipei*
[27]*H. Niewodniczanski Institute of Nuclear Physics, Krakow*
[28]*Nippon Dental University, Niigata*
[29]*Niigata University, Niigata*
[30]*University of Nova Gorica, Nova Gorica*
[31]*Osaka City University, Osaka*
[32]*Osaka University, Osaka*
[33]*Panjab University, Chandigarh*
[34]*Saga University, Saga*

[35]University of Science and Technology of China, Hefei
[36]Seoul National University, Seoul
[37]Sungkyunkwan University, Suwon
[38]University of Sydney, Sydney, New South Wales
[39]Toho University, Funabashi
[40]Tohoku Gakuin University, Tagajo
[41]Tohoku University, Sendai
[42]Department of Physics, University of Tokyo, Tokyo
[43]Tokyo Institute of Technology, Tokyo
[44]Tokyo Metropolitan University, Tokyo
[45]Tokyo University of Agriculture and Technology, Tokyo
[46]Virginia Polytechnic Institute and State University, Blacksburg, Virginia 24061
[47]Yonsei University, Seoul
(Received 18 September 2007; published 18 January 2008)

We report the first measurement of CP-violation parameters in $B^0 \to \rho^0\gamma$ decays based on a data sample of $657 \times 10^6 B\bar{B}$ pairs collected with the Belle detector at the KEKB asymmetric-energy e^+e^- collider. We obtain the time-dependent and direct CP-violating parameters, $\mathcal{S}_{\rho^0\gamma} = -0.83 \pm 0.65(\text{stat}) \pm 0.18(\text{syst})$ and $\mathcal{A}_{\rho^0\gamma} = -0.44 \pm 0.49(\text{stat}) \pm 0.14(\text{syst})$, respectively.

DOI: 10.1103/PhysRevLett.100.021602 PACS numbers: 13.20.He, 11.30.Er

Radiative decay processes are sensitive to physics beyond the standard model (SM). Figure 1 shows the lowest order Feynman diagram for radiative b decay in the SM. The heavy SM particles in the loop can be replaced by new physics (NP) particles. Hence the corresponding physics observables may deviate from SM expectations. Recently, the possibility of time-dependent CP asymmetries in $b \to s\gamma$ from NP have drawn much theoretical and experimental interest [1–4]. Both Belle [3] and *BABAR* [4] have measured time-dependent CP-violating parameters in $B^0 \to K^0_S\pi^0\gamma$ decay. The results so far are consistent with the SM.

Signals for $B^0 \to \rho^0\gamma$ have been established by Belle [5] and *BABAR* [6], which enables us to measure CP asymmetries in the $b \to d\gamma$ process. As in $b \to s\gamma$, the photon emitted in $b \to d\gamma$ ($\bar{b} \to \bar{d}\gamma$) is predominantly left handed (right handed), and hence the final state is flavor specific [1]. In the decay $B^0 \to \rho^0\gamma$, the SM predicts no time-dependent CP asymmetry ($\mathcal{S}$) and -0.1 for the direct CP asymmetry ($\mathcal{A}$) [2,7]. In particular, assuming the top quark is the dominant contribution in the loop shown in Fig. 1, the decay amplitude has a weak phase ϕ_1 that cancels the phase in the mixing; consequently $\mathcal{S}$ vanishes. Observing a nonzero value of $\mathcal{S}$ would indicate effects of NP [8]. In this Letter, we present the first measurements of $\mathcal{S}$ and $\mathcal{A}$ for the $B^0 \to \rho^0(\to \pi^+\pi^-)\gamma$ transition based on $657 \times 10^6 B\bar{B}$ pairs collected with the Belle detector [9] at the KEKB asymmetric-energy e^+e^- (3.5 on 8.0 GeV) collider [10].

The Belle detector is a large-solid-angle magnetic spectrometer that consists of a silicon vertex detector (SVD), a 50-layer central drift chamber, an array of aerogel threshold Cherenkov counters, a barrel-like arrangement of time-of-flight scintillation counters, and an electromagnetic calorimeter (ECL) comprised of CsI(Tl) crystals located inside a superconducting solenoid coil that provides a 1.5 T magnetic field. An iron flux return located outside of the coil is instrumented to detect K^0_L mesons and to identify muons.

At the KEKB, the $\Upsilon(4S)$ is produced with a Lorentz boost of $\beta\gamma = 0.425$ along the z axis, which is defined as the direction antiparallel to the e^+ beam direction. In the decay chain $\Upsilon(4S) \to B^0\bar{B}^0 \to f_{\text{rec}}f_{\text{tag}}$, where one of the B mesons decays at time t_{rec} to a final state f_{rec}, which is our signal mode, and the other decays at time t_{tag} to a final state f_{tag} that distinguishes between B^0 and $\bar{B}^0$, the decay rate has a time dependence given by

$$\mathcal{P}(\Delta t) = \frac{e^{-|\Delta t|/\tau_{B^0}}}{4\tau_{B^0}}\{1 + q[\mathcal{S}\sin(\Delta m_d \Delta t) + \mathcal{A}\cos(\Delta m_d \Delta t)]\}. \quad (1)$$

Here τ_{B^0} is the B^0 lifetime, Δm_d is the mass difference between the two B^0 mass eigenstates, Δt is the time difference $t_{\text{rec}} - t_{\text{tag}}$, and the b-flavor charge $q = +1(-1)$ when the tagging B meson is a B^0 ($\bar{B}^0$). Since the B^0 and $\bar{B}^0$ mesons are approximately at rest in the $\Upsilon(4S)$ center-of-mass system (c.m.s.), Δt can be determined from the displacement in z between the f_{rec} and f_{tag} decay vertices: $\Delta t \simeq (z_{\text{rec}} - z_{\text{tag}})/(\beta\gamma c) \equiv \Delta z/(\beta\gamma c)$.

We reconstruct $B^0 \to \rho^0\gamma$, as well as a control sample of $B^0 \to K^{*0}(\to K^+\pi^-)\gamma$ [11]. For high energy prompt pho-

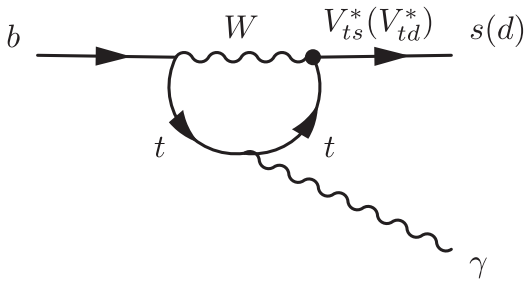

FIG. 1. Feynman diagram for radiative b decay in the SM.

tons, we select the cluster in the ECL with the highest energy in the c.m.s. from clusters that have no associated charged track. We require 1.4 GeV $< E_\gamma^{\mathrm{c.m.s.}} <$ 3.4 GeV. For the selected photon, we also require $E_9/E_{25} > 0.95$, where E_9/E_{25} is the ratio of energies summed in 3×3 and 5×5 arrays of CsI(Tl) crystals around the center of the shower. In order to reduce the background from $\pi^0 \to \gamma\gamma$ or $\eta \to \gamma\gamma$ decays, photons from these decays are rejected as described in [12]; this retains 97% of the signal and rejects 20% of the background events. The polar angle of the photon direction in the laboratory frame is restricted to the barrel region of the ECL ($33° < \theta_\gamma < 128°$).

Charged tracks are required to originate from the vicinity of the interaction point (IP), within 3 cm in z and 0.5 cm in r-ϕ; their transverse momenta are required to be greater than 0.22 GeV/c. Charged tracks from K_S^0 decays as well as positively identified protons, muons, and electrons are excluded. Finally, candidate tracks are classified as pion candidates and kaon candidates according to the ratio of kaon and pion particle identification likelihoods. This selection retains 87% of pions while rejecting 92% of kaons. Pairs of oppositely charged pions are combined to form ρ^0 candidates. Oppositely charged kaon and pion candidates are combined to form K^{*0} candidates. We form the invariant mass $M_{K\pi}$ for K^{*0} and ρ^0 candidates. To obtain $M_{K\pi}$ for ρ^0 candidates, we assign the kaon mass to each pion in turn and take the lower of the two values. We use $M_{K\pi}$ rather than $M_{\pi\pi}$ since it gives a better separation of the $\rho^0\gamma$ signal from the $K^{*0}\gamma$ background.

We form two kinematic variables: the energy difference $\Delta E \equiv (\sum_i E_i^*) - E_{\mathrm{beam}}^*$ and the beam-energy constrained mass $M_{\mathrm{bc}} \equiv \sqrt{(E_{\mathrm{beam}}^*)^2 - (\sum_i p_i^*)^2}$, where E_{beam}^* is the beam energy in the c.m.s., E_i^* and p_i^* are the energy and momentum of the ith final state particle in the c.m.s., and the summation is taken over all the final state particles of the candidate B meson. Unlike $M_{K\pi}$, we do not assign the kaon mass but instead assign the pion mass to form the energy and the momentum of $\rho^0\gamma$ candidates. The signal box in ΔE, M_{bc}, and $M_{K\pi}$, which is used for the measurements of CP-violating parameters, is defined as -0.15 GeV $\le \Delta E \le 0.1$ GeV, 5.27 GeV/$c^2 \le M_{\mathrm{bc}} \le$ 5.29 GeV/c^2, and 0.7 GeV/$c^2 < M_{K\pi} <$ 1.1 GeV/c^2. A larger region in ΔE and M_{bc}, -0.3 GeV $< \Delta E <$ 0.5 GeV and 5.2 GeV/$c^2 < M_{\mathrm{bc}}$, is used to determine the signal and background fractions.

In order to suppress the background contribution from $q\bar{q}$ ($e^+e^- \to q\bar{q}$ with $q = u, d, s, c$), an event likelihood ratio $\mathcal{R}$ is formed from likelihood variables for signal ($\mathcal{L}_{\mathrm{sig}}$) and background ($\mathcal{L}_{\mathrm{bkg}}$) as $\mathcal{R} \equiv \mathcal{L}_{\mathrm{sig}}/(\mathcal{L}_{\mathrm{sig}} + \mathcal{L}_{\mathrm{bkg}})$. These likelihood variables are obtained by combining three variables: a Fisher discriminant $\mathcal{F}$ [13] that uses modified Fox-Wolfram moments [14] as discriminating variables, the polar angle of the B meson candidate momentum in the c.m.s. ($\cos\theta_B$), and the cosine of the helicity angle ($\cos\theta_H$) defined as the momentum direction of the π^+ with respect to the opposite of the B momentum in the ρ^0 rest frame (similarly for $K^{*0}\gamma$). We also require $|\cos\theta_H| < 0.75$ in order to suppress background from random low momentum pions. $\mathcal{R}$ is also used to determine the best candidate when multiple candidates are found in a single event, although the fraction of events with multiple candidates is small (0.7%).

There is a large background from $B^0 \to K^{*0}\gamma$, which has a branching fraction 40 times larger than that of $B^0 \to \rho^0\gamma$. When a kaon is misidentified as a pion, the $K^{*0}\gamma$ events easily mimic the $\rho^0\gamma$ signal. This background peaks at K^{*0} mass in $M_{K\pi}$ and distributes in low ΔE region because the pion mass is assigned to the kaon. However, this is still acceptable since the CP asymmetries in the $B^0 \to K^{*0}\gamma$ decay are known with good precision. There are several background contributions from B decays that could have finite CP asymmetries, $\rho^+\pi^-$, $\rho^0\pi^0$, and $\pi^+\pi^-\eta$; however, the contributions from these modes are small and thus their impact on our measurement is tiny.

The b flavor of the accompanying B meson is identified from inclusive properties of particles that are not associated with the reconstructed signal decay. The algorithm for flavor tagging is described in detail elsewhere [15]. We use two parameters, q defined in Eq. (1) and r, to represent the tagging information. The parameter r is an event-by-event flavor-tagging quality factor that ranges from 0 to 1: $r = 0$ when there is no flavor discrimination and $r = 1$ when the flavor assignment is unambiguous. The value of r is determined by using Monte Carlo (MC) simulations and is used to sort data into seven r intervals. Events with $r > 0.1$ are sorted into six r intervals; for each interval, the wrong-tag fraction w and the difference Δw in w between the B^0 and $\bar{B}^0$ decays are determined from high-statistics control samples of semileptonic and hadronic $b \to c$ decays. For events with $r \le 0.1$, there is negligible flavor discrimination available and we set w to 0.5.

The vertex position of the signal-side decay of $B^0 \to \rho^0\gamma$ and the control sample $B^0 \to K^{*0}\gamma$ is reconstructed from one or two charged track trajectories that have enough hits in the SVD, with a constraint on the IP. The IP profile ($\sigma_x \simeq 100$ μm, $\sigma_y \simeq 5$ μm) is smeared by the finite B flight length in the plane perpendicular to the z axis (21 μm). The other (tag-side) B vertex is determined from well reconstructed tracks that are not assigned to the signal-side. A constraint to the IP profile is also imposed. The resolution of the distance of the two B vertices is typically 160 μm.

After all the selections are applied, we obtain 5362 candidates in the ΔE-M_{bc}-$M_{K\pi}$ fit region, of which 410 are in the signal box. We perform an extended unbinned maximum likelihood (UML) fit to the ΔE-M_{bc}-$M_{K\pi}$ distribution in order to resolve the $\rho^0\gamma$, $K^{*0}\gamma$, other $B\bar{B}$ and $q\bar{q}$ components.

The probability density function (PDF) for $\rho^0\gamma$ and $K^{*0}\gamma$ are obtained from MC simulations. We use a two-dimensional histogram for M_{bc}-ΔE and two one-dimensional histograms for $M_{K\pi}$ depending on ΔE. For

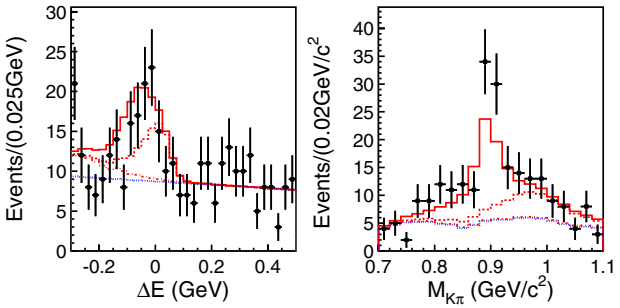

FIG. 2 (color online). ΔE (left) and $M_{K\pi}$ (right) distributions for signal enhanced samples. The following selections are applied: $5.27\ \mathrm{GeV}/c^2 \le M_{\mathrm{bc}} \le 5.29\ \mathrm{GeV}/c^2$ and $0.92\ \mathrm{GeV}/c^2 \le M_{K\pi}$ (left); $5.27\ \mathrm{GeV}/c^2 \le M_{\mathrm{bc}} \le 5.29\ \mathrm{GeV}/c^2$ and $-0.05\ \mathrm{GeV} \le \Delta E \le 0.1\ \mathrm{GeV}$ (right). Points with error bars are data. The solid histograms show the fit results. The areas divided by lines show the breakdown; from top to bottom, $B^0 \to K^{*0}\gamma$, $B^0 \to \rho^0\gamma$, and other $B\bar{B}$ and $q\bar{q}$ components. Note that the other $B\bar{B}$ component is too small to be visible in the plot on the right.

these PDFs, the peak position and the width are corrected using the $B^0 \to K^{*0}\gamma$ control sample in order to account for differences between data and simulation. The PDF for the other $B\bar{B}$ background component, which populates the lower ΔE region, is also obtained from MC simulations. For $q\bar{q}$ background, we use the product of one-dimensional PDFs: the ARGUS parameterization [16] for M_{bc}, a first-order polynomial for ΔE, and a 20 bin histogram for $M_{K\pi}$. The shape parameters (one ARGUS coefficient, one polynomial coefficient, and fractions of 19 bin contents) are determined in the fit. Together with the yield of the four components, we have 25 free parameters in the fit.

From the fit, we find 48.3 ± 13.5 $\rho^0\gamma$ candidates, 180.6 ± 16.8 $K^{*0}\gamma$ background candidates, 10.3 ± 4.3 other $B\bar{B}$ background candidates, and 168.8 ± 2.6 $q\bar{q}$ background candidates inside the signal box. Figure 2 shows the ΔE and $M_{K\pi}$ projections of the fit result for the signal enhanced samples. The observed $M_{K\pi}$ distribution is described well by our PDF, which implies there is no significant contribution from nonresonant $\pi^+\pi^-\gamma$ or $K^+\pi^-\gamma$.

We determine $\mathcal{S}$ and $\mathcal{A}$ from a UML fit to the observed Δt distribution. For each event, the following likelihood function is evaluated:

$$P_i = (1 - f_{\mathrm{ol}}) \int_{-\infty}^{+\infty} d(\Delta t') \left[\sum_j f_j \mathcal{P}_j(\Delta t') R_j(\Delta t_i - \Delta t') \right] + f_{\mathrm{ol}} P_{\mathrm{ol}}(\Delta t_i), \quad (2)$$

where j runs over four components ($B^0 \to \rho^0\gamma$, $B^0 \to K^{*0}\gamma$, other $B\bar{B}$ and $q\bar{q}$). The probability of each component (f_j) is calculated using the result of the M_{bc}-ΔE-$M_{K\pi}$ fit on an event-by-event basis. We also incorporate the flavor-tagging quality r distribution. The r distributions for $K^{*0}\gamma$ and $q\bar{q}$ are obtained by repeating the M_{bc}-ΔE-$M_{K\pi}$ fit procedure to the signal sample and also to the control sample for each r interval with yield parameters floated. We found consistent distributions for the signal sample and the control sample. The r distribution for $\rho^0\gamma$ is expected to be consistent with $K^{*0}\gamma$, since the flavor is determined only by the tag side; this is confirmed by MC simulations. The distribution of $B\bar{B}$ background is estimated from MC simulations.

The PDF expected for the $\rho^0\gamma$ distribution, $\mathcal{P}_{\rho^0\gamma}$, is given by the time-dependent decay rate [Eq. (1)], modified to incorporate the effect of incorrect flavor assignment; the parameters τ_{B^0} and Δm_d are fixed to their world-average values [17]. The distribution is then convolved with the proper-time interval resolution function $R_{\rho^0\gamma}$, which takes into account the finite vertex resolution. The parametrization of $R_{\rho^0\gamma}$ is the same as the one used in the $B^0 \to \phi K^0$ [18] analysis. The same functional forms for the PDF and resolution are used for the $K^{*0}\gamma$ and other $B\bar{B}$ components, but with separate lifetime and CP-violating parameters. We assume no CP asymmetry in $K^{*0}\gamma$ and other $B\bar{B}$ background events; possible deviations from this assumption are taken into account in the systematic error. The lifetime of $B^0 \to K^{*0}\gamma$ is the same as $B^0 \to \rho^0\gamma$. The effective lifetime of $B\bar{B}$ background is obtained from a fit to the MC sample; the result is 1.26 ± 0.06 ps. The PDF for $q\bar{q}$ background events, $\mathcal{P}_{q\bar{q}}$, is modeled as a sum of exponential and delta function components and is convolved with a double Gaussian which represents the resolution function $R_{q\bar{q}}$. All parameters in $\mathcal{P}_{q\bar{q}}$ and $R_{q\bar{q}}$ are determined by a fit to the Δt distribution in the ΔE-M_{bc} sideband region [$\Delta E > 0.2$ or $25(M_{\mathrm{bc}} - 5.26) < (\Delta E - 0.2)$ with ΔE in GeV and M_{bc} in GeV/c^2]. P_{ol} is a Gaussian function that represents a small outlier component with fraction f_{ol} [19].

The only free parameters in the CP fit to $B^0 \to \rho^0\gamma$ are $\mathcal{S}_{\rho^0\gamma}$ and $\mathcal{A}_{\rho^0\gamma}$, which are determined by maximizing the likelihood function $L = \prod_i P_i(\Delta t_i; \mathcal{S}, \mathcal{A})$, where the product is over all events. We obtain

$$\mathcal{S}_{\rho^0\gamma} = -0.83 \pm 0.65(\mathrm{stat}) \pm 0.18(\mathrm{syst}), \quad (3)$$

and

$$\mathcal{A}_{\rho^0\gamma} = -0.44 \pm 0.49(\mathrm{stat}) \pm 0.14(\mathrm{syst}), \quad (4)$$

where the systematic errors are obtained as discussed below.

We define the raw asymmetry in each Δt bin by $(N_{q=+1} - N_{q=-1})/(N_{q=+1} + N_{q=-1})$, where $N_{q=+1(-1)}$ is the number of observed candidates with $q = +1(-1)$. Figure 3 shows the Δt distributions and the raw asymmetry for events with $0.5 < r \le 1.0$.

We perform various validity checks of our fitting procedure. A lifetime fit for the $B^0 \to K^{*0}\gamma$ control sample, the $K^{*0}\gamma$ component in the $B^0 \to \rho^0\gamma$ sample, and the $\rho^0\gamma$ candidates gives 1.57 ± 0.04 ps, 1.54 ± 0.16 ps, and $1.26^{+0.37}_{-0.30}$ ps, respectively. These results are all consistent

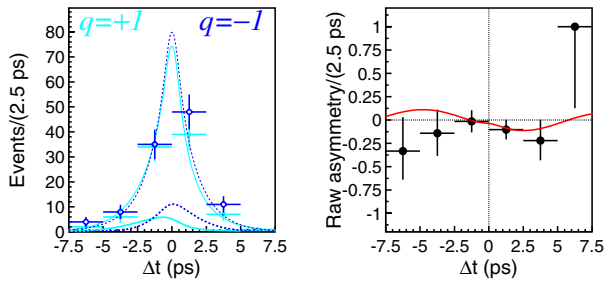

FIG. 3 (color online). (Left) Δt distributions for $B^0 \to \rho^0\gamma$ for $q = +1$ (light solid line) and $q = -1$ (dark dashed line) with $0.5 < r \leq 1.0$. The thin curve is the fit projection while the thick curve shows the signal component. Points with error bars are data. (Right) Raw asymmetry in each Δt bin with $0.5 < r \leq 1.0$. The solid curve shows the result of the UML fit.

with the nominal B^0 lifetime (1.530 ± 0.009 ps [17]). A CP asymmetry fit for the control sample gives an asymmetry consistent with zero ($\mathcal{S} = +0.05 \pm 0.07$, $\mathcal{A} = -0.01 \pm 0.05$). A CP asymmetry fit to the $K^{*0}\gamma$ component in the $B^0 \to \rho^0\gamma$ sample also gives a consistent result ($\mathcal{S} = +0.02 \pm 0.25$, $\mathcal{A} = -0.03 \pm 0.17$).

We evaluate systematic uncertainties in the following categories by fitting the data with each fixed parameter shifted by its 1σ error. The largest contribution to the systematic error is from the uncertainty in the probability of each component (f_j) because of the limited statistics; we find an uncertainty of 0.16 on $\mathcal{S}$ and 0.09 on $\mathcal{A}$. The CP asymmetry in $K^{*0}\gamma$ has a direct impact on the measurement. Based on the fit result from the control sample, we vary $\mathcal{A}_{K^{*0}\gamma}$ from zero up to ± 0.05 and find an error of 0.04 on $\mathcal{A}$. The CP asymmetry in other $B\bar{B}$ backgrounds has less impact on the measurement. This asymmetry is varied by the weighted average of possible maximum CP asymmetries (± 1 if not measured) of contributing decay modes (0.06 on $\mathcal{S}$, 0.09 on $\mathcal{A}$); we find an error of 0.01 or less on both $\mathcal{S}$ and $\mathcal{A}$. The uncertainty from the resolution function parameters is 0.06 on $\mathcal{S}$ and 0.07 on $\mathcal{A}$. In addition to the above-mentioned categories, we also take the following small sources of uncertainty into account: the uncertainty in the vertex reconstruction and flavor tagging, uncertainty due to the tag-side interference effect [20], uncertainty in the knowledge of the $q\bar{q}$ background Δt PDF, uncertainty in the physics parameters such as Δm_d, τ_{B^0}, possible effect of correlations between $M_{\rm bc}$, ΔE, and $M_{K\pi}$, and other possible biases. Adding these contributions in quadrature, we obtain a systematic error of 0.18 on $\mathcal{S}$ and 0.14 on $\mathcal{A}$.

In summary, we have measured the time-dependent CP asymmetry in the decay $B^0 \to \rho^0\gamma$ using a sample of $657 \times 10^6 B\bar{B}$ pairs. We obtain CP-violation parameters $\mathcal{S}_{\rho^0\gamma} = -0.83 \pm 0.65(\text{stat}) \pm 0.18(\text{syst})$ and $\mathcal{A}_{\rho^0\gamma} = -0.44 \pm 0.49(\text{stat}) \pm 0.14(\text{syst})$. With the present statistics, the result is consistent with no CP asymmetry and therefore no indication of NP is found. This is the first measurement of CP asymmetry parameters in a $b \to d\gamma$ process.

We thank the KEKB group for excellent operation of the accelerator, the KEK cryogenics group for efficient solenoid operations, and the KEK computer group and the NII for valuable computing and Super-SINET network support. We acknowledge support from MEXT and JSPS (Japan); ARC and DEST (Australia); NSFC and KIP of CAS (China); DST (India); MOEHRD, KOSEF and KRF (Korea); KBN (Poland); MES and RFAAE (Russia); ARRS (Slovenia); SNSF (Switzerland); NSC and MOE (Taiwan); and DOE (USA).

[1] D. Atwood, M. Gronau, and A. Soni, Phys. Rev. Lett. **79**, 185 (1997).
[2] P. Ball, G. W. Jones, and R. Zwicky, Phys. Rev. D **75**, 054004 (2007).
[3] Y. Ushiroda *et al.* (Belle Collaboration), Phys. Rev. D **74**, 111104 (2006).
[4] B. Aubert *et al.* (*BABAR* Collaboration), Phys. Rev. D **72**, 051103 (2005).
[5] D. Mohapatra *et al.* (Belle Collaboration), Phys. Rev. Lett. **96**, 221601 (2006).
[6] B. Aubert *et al.* (*BABAR* Collaboration), Phys. Rev. Lett. **98**, 151802 (2007).
[7] A. Ali, E. Lunghi, and A. Y. Parkhomenko, Phys. Lett. B **595**, 323 (2004); C. D. Lu, M. Matsumori, A. I. Sanda, and M. Z. Yang, Phys. Rev. D **72**, 094005 (2005); **73**, 039902(E) (2006).
[8] C. S. Kim, Y. G. Kim, and K. Y. Lee, Phys. Rev. D **71**, 054014 (2005).
[9] A. Abashian *et al.* (Belle Collaboration), Nucl. Instrum. Methods Phys. Res., Sect. A **479**, 117 (2002).
[10] S. Kurokawa and E. Kikutani, Nucl. Instrum. Methods Phys. Res., Sect. A **499**, 1 (2003) and other papers included in this volume.
[11] All decay modes include the charge conjugate, unless otherwise stated.
[12] P. Koppenburg *et al.* (Belle Collaboration), Phys. Rev. Lett. **93**, 061803 (2004).
[13] R. A. Fisher, Annals Eugen. **7**, 179 (1936).
[14] K. Abe *et al.* (Belle Collaboration), Phys. Rev. Lett. **91**, 261801 (2003).
[15] H. Kakuno and K. Hara *et al.*, Nucl. Instrum. Methods Phys. Res., Sect. A **533**, 516 (2004).
[16] H. Albrecht *et al.* (ARGUS Collaboration), Phys. Lett. B **241**, 278 (1990).
[17] W.-M. Yao *et al.* (Particle Data Group), J. Phys. G **33**, 1 (2006).
[18] K. F. Chen *et al.* (Belle Collaboration), Phys. Rev. Lett. **98**, 031802 (2007).
[19] H. Tajima *et al.*, Nucl. Instrum. Methods Phys. Res., Sect. A **533**, 370 (2004).
[20] O. Long, M. Baak, R. N. Cahn, and D. Kirkby, Phys. Rev. D **68**, 034010 (2003).